

Physical chemistry of acridine adsorption onto gold surface: The influence of nanostructure as revealed by near-infrared and tip-enhanced Raman spectroscopy (TERS)

Roman M. Balabin^a, Thomas Schmid^a, Rustem Z. Syunyaev^b, and Renato Zenobi^{*a}

^a Department of Chemistry and Applied Biosciences, ETH Zurich, 8093 Zurich, Switzerland

^b Gubkin Russian State University of Oil and Gas, 119991 Moscow, Russia

ABSTRACT

We report a detailed study of adsorption of acridine and a number of its derivatives: benz[a]acridine, benz[c]acridine, etc. Thermodynamic and kinetic data, obtained by solution-phase near-infrared spectroscopy (NIRS), clearly show a great difference of adsorption behavior for flat and nanorough (app. 4 nm) gold surfaces. Gibbs free energies and adsorption kinetic constants were determined for flat and SERS-type surfaces. The characterization of the polyaromatic monolayer directly at the Au surface, as measured by tip-enhanced Raman spectroscopy in scanning tunneling microscope mode (STM-TERS), has confirmed the dependence of the adsorption parameters on the (nano)roughness of the metal surface.

Keywords: catalysis, gold nanoparticles (AuNPs), adsorption, aromatic/heteroaromatic molecules (petroleum resins/asphaltenes), metals (Au, Ag, Cu, Pt, Pd), near-infrared spectroscopy (NIR/NIRS), atomic force microscopy (AFM), scanning tunneling microscopy (STM), Raman microscopy, surface enhanced Raman spectroscopy (SERS)

1. INTRODUCTION

Heterogeneous catalysts lie at the heart of many processes in the chemical industry [1]. These catalysts are typically composed of metal nanoparticles that are dispersed across the surface of a support material. There are several benefits of reducing the size of the catalyst particles to the nanoscale, the most obvious being that the specific surface area at which catalytic action can take place increases. Moreover, the surface structure and electronic properties of the particle can change in ways that improve catalytic performance [1-20].

The benefits of moving to the nanoscale are perhaps best illustrated by gold. In its bulk form gold is relatively chemically inert, but in nanoparticle form it becomes active for a range of important catalytic reactions, from the oxidation of carbon monoxide to diesel soot combustion [21-37]. In other words, the recent interest in the structure and reactivity of small gold and silver clusters, both experimentally and theoretically, has been driven by the unique uses of these clusters [38-59]. Supported gold nanoparticles (AuNP) have created much excitement owing to their unusual and somewhat unexpected catalytic properties, which are still not fully understood [22]. The adsorption of molecular species to gold or silver neutral, cationic, or anionic clusters is the first step in any heterogeneous catalytic process [11].

Further author information: (Send correspondence to R.Z.)

R.Z.: E-mail: zenobi@org.chem.ethz.ch, Telephone: +41-44-632-4376

It is commonly accepted that the size dependence is the key issue for catalysis by Au particles [23]. Effective control of the dispersion and size of supported gold particles is thus a primary goal of catalyst design, but this is quite challenging. For example, experimental work on gold particles supported on a titanium dioxide (110) single-crystal surface established a striking size threshold effect associated with a metal-to-insulator transition, with gold particles catalytically active only if their diameters are below 3.5 nm [24]. In 2008 it was shown [22] that very small gold entities (~1.4 nm) derived from 55-atom gold clusters and supported on inert materials (boron nitride, silicon dioxide or carbon) are efficient and robust catalysts for the selective oxidation of styrene to benzaldehyde, styrene epoxide, and acetophenone by dioxygen (O₂) in toluene solvent. Au₅₅-derived catalysts supported on SiO₂ exhibited turnover frequencies of ~0.03 s⁻¹ for styrene conversion and ~0.003 s⁻¹ for epoxide production. A sharp size threshold in catalytic activity was also found, in that particles with diameters of 2 nm and above are completely inactive. These observations (including X-ray photoelectron spectra) suggest that catalytic activity arises from the altered electronic structure intrinsic to small gold nanoparticles [22]. It was also shown that extremely small Au nanoparticles supported on chemically and electronically inert materials can adsorb and activate O₂ for selective oxidation [11-15,25-32].

Since a direct contact between reagent and catalyst is one of the main steps of any heterogeneous catalytic reaction [33,34], there is a direct link between adsorption behavior and catalytic activity. In many cases the change of catalytic activity can be explained by the change of adsorption behavior of reactants, intermediates, or products [17,33-35]. For example, the adsorption of CO on Au surfaces is one of the important steps in CO oxidation. Boccuzzi et al. [36] have found that an Au/TiO₂ catalyst prepared by deposition-precipitation contains three different Au sites for CO adsorption depending on the pretreatment conditions: CO adsorbed linearly on metallic Au sites, but it is bridge-bonded to small Au clusters perturbed by the negative charge [37]. For the same reaction [38] a size dependency of CO adsorption was observed from studying size-selected Au anion clusters: the highest reactivity of CO was observed for the anion clusters of 11 atoms [39].

In one of the recently reported works, Haruta and co-workers [40,41] remarkably showed a better performance of gold clusters of <2 nm compared to silver- and copper-based catalytic systems by using O₂/H₂O as oxidant of propylene. Although the yield is still very low, the selectivity was >50%. Spectroscopic evidence for the adsorption of propene on gold nanoparticles during hydroepoxidation has been observed [42], and an experimental and theoretical study of the catalytic activity of soft-landed subnanometer gold clusters (Au₆-Au₁₀) has been performed [43], as well as model calculations on the oxidation over Au(111) surfaces [44].

Recent interest in gold-catalysed chemistry of aromatic/heteroaromatic substances (including nitroarene reduction with imine formation [45]; catalytic oxidation of benzene, toluene and p-xylene over colloidal gold of ~3 nm [22,46]; cross-coupling of phenylacetylene and iodobenzene with ~20 nm gold particles [47]; the three-component coupling reaction of benzaldehyde, piperidine, and phenylacetylene [48]) puts a question of the role of the substrate/catalyst nanoroughness onto the observed catalytic activity [49-51].

In this work we explore the adsorption of heteroaromatic molecules onto gold surfaces of different roughness by combination of near-infrared (NIR) and tip-enhanced Raman spectroscopy (TERS). We find a striking difference between acridine adsorption behavior on flat and nanorough surfaces. We try to answer the question: what leads to the difference observed? We propose and prove that surface nanoroughness leads to a change in the adsorption mode of acridine: from adsorption via the π -electron system to adsorption via the nitrogen lone-pair.

2. EXPERIMENTAL

The homebuilt near infrared (NIR) setup [52] consisted of a hermetic glass cell (1.5×1.0×1.0 cm) and three NIR optical fibers. Each fiber led to a separate homemade spectrometer. Such a configuration enables us to monitor solution concentrations at three different heights, ensuring that no sedimentation or phase separation occurs during the adsorption process. It also increases the amount of signal per time unit by a factor of three. Identical halogen incandescent lamps were used as light sources and identical silicon photodiodes were used as detectors in the Fourier transform near infrared spectrometers (FT-NIR). See Ref.[52] for a detailed discussion of the experimental setup.

The spectral region of 9000-13000 cm^{-1} (1111-769 nm) was scanned with a resolution of 8 cm^{-1} (24 scans) [52-54]. A photometric accuracy of 0.022% (transmittance) was reached for a collection time of 2.6 s (excluding the time for FT analysis). The optical path length was fixed to 1.0 cm.

The frequency region scanned combines the advantages (selectivity / chemical information content) of vibrational spectroscopy (overtones of fundamental bands are observed in NIR) with the technical simplicity and low cost of absorption spectroscopy in the visible range. For these reasons, NIR is an attractive technique for modern physical chemistry and surface science. In particular, NIR spectroscopic measurements allow to differentiate chemical structures by their vibrational overtones [3], a feature that is not observed in reflectivity measurements, where all chemical substances can influence the observed signal change (e.g., refractive index change). The NIR technique has proven its effectiveness when analysing extremely complex petroleum systems like resins and asphaltenes [52-54].

An upright Raman microscope (NTEGRA Spectra, NT-MDT, Russia) was employed for Raman microscopy and AFM/STM measurements [55]. The system is equipped with an upright confocal laser microscope, an atomic force microscope (AFM), a white-light video microscope for rough observation/alignment of the sample, a photomultiplier tube (PMT) detector for confocal imaging, and a Raman spectrograph equipped with a charge-coupled device (CCD). It allows simultaneous AFM/STM and optical measurements on exactly the same part of transparent and opaque samples. All optical measurements were performed using a 100× long working-distance objective with a numerical aperture (NA) of 0.7 for both, excitation and collection of the backscattered light from the sample. Two lasers, a red HeNe laser (632.8 nm, 5 mW at the sample from Laser Drive, Inc.) and a green DPSS laser (532 nm, 3-4 mW at the sample from Changchun New Industries (CNI) Optoelectronics Tech. Co., Ltd.; China) were used for Raman microscopy and spectroscopy. The HeNe laser was used for the TERS measurements.

The STM-TERS instrument consists of a 100×100×10 μm piezo scanner for sample movement, controlled by an STM feedback unit, and allows full visibility of tip and sample simultaneously [55]. The tip is held at a 30-50° angle with respect to the sample surface, can be positioned laterally, and is approached by moving the sample into tunneling contact. The STM tip holder unit was custom designed to fulfill these needs [55]. Light emitted or scattered from the sample is collected by the same optics, separated by an edge filter, and directed into a quadruple grating Raman spectrometer (integral part of the NT-MDT system). The photons from the selected part of the spectrum are then acquired by an electron multiplying CCD (EMCCD), which is Peltier cooled to -90 °C (Andor, Newton 971) [55].

Acridine (>97%, Sigma-Aldrich), benz[a]acridine (BCR157, Fluka), and benz[c]acridine (BCR158, Fluka) were used without further purification. Benzene (>99.5%, Fluka) and anhydrous ethanol ($\geq 99.8\%$, Fluka, puriss. p.a., ACS reagent) were used as solvents without further purification. The simplicity of the benzene NIR spectrum in the desired region (just one peak) ensures an accurate evaluation of the solute concentration. The use of simple aromatic solvents is popular in catalysis by AuNP [22,45-51]. Two types of gold surfaces were prepared by vapor coating (Bal-Tec MED 020) 50 and 4 nm of gold onto glass slides to produce relatively flat and rough surfaces, respectively [55]. The flatness/roughness of the gold layer was checked by AFM/STM and scanning electron microscopy (SEM). The 4-nm

nanorough surface has an average gold cluster XY-size of 4.2 ± 2.5 nm with a height of 3.1 ± 0.9 nm (RMS roughness); the 50-nm flat one has an average grain size of 21 ± 5 nm with a height of 9.5 ± 1.7 nm (RMS roughness). An atomically flat gold surface, prepared according to Ref.[55], was used to validate the flat results. The surface area of all adsorbents was measured by the BET method [56]; it was used to normalize the adsorbed mass and calculate the adsorbed mass density in $[\text{mg m}^{-2}]$.

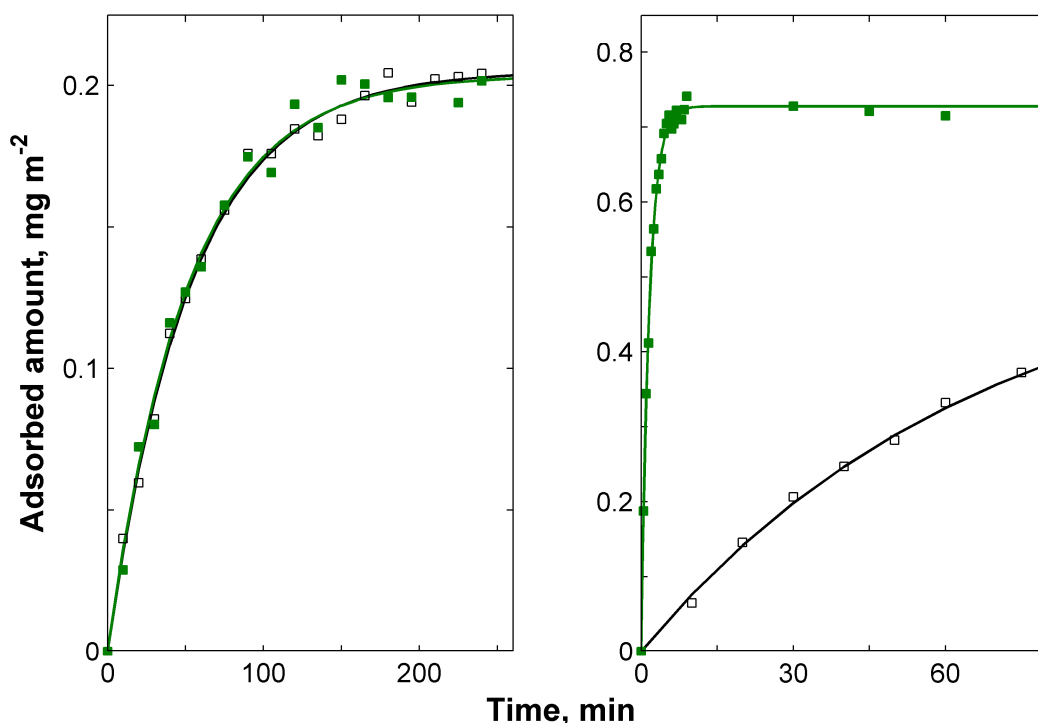


Figure 1. Kinetics of acridine adsorption from (left) ethanol and (right) benzene solutions onto (black, empty) flat or (green, filled) nanorough Au surfaces. The data were measured by near-infrared (NIR) spectroscopy. The experimental data points were fitted with a Langmuir (exponential) kinetic model. Note the difference in the X-axis (time) scale.

The AFM/STM and Raman measurements were controlled by NT-MDT's Nova software. MATLAB 2010b (MathWorks, USA) was used for data analysis. The MATLAB Curve Fitting Toolbox was used for curve fitting. The MATLAB iToolbox was used for building of a partial least squares (PLS) calibration model. The PLS regression method was used for concentration evaluation from NIR spectroscopic data [57]. The PLS method finds a linear model by projecting the predicted variables (Y, concentrations) and the observable variables (X, spectra) to a new space. It is used to find the fundamental relation between two matrices (X and Y), i.e. a latent variable approach to modeling the covariance structure in these two spaces. A PLS model will try to find the multidimensional direction in the X space that explains the maximum multidimensional variance direction in the Y space. PLS-regression is particularly suited when the matrix of predictors has more variables than observations, and when there is multicollinearity among X values (e.g., spectral data). The method has proven its efficiency (when compared with classical regression models) in NIR data analysis [57].

The PLS model was built using 74 spectra of acridine solutions in ethanol or benzene with concentrations from 0 to 500 mg L⁻¹. The resulting model (3 latent variables) has an accuracy (root mean squared error of prediction – RMSEP) of 0.022 mg L⁻¹. All experiments were conducted 7 times. The 5 best points were used for averaging [58]. More sophisticated multivariate regression methods, based on principal component analysis – artificial neural networks (ANNs), support vector machines (SVMs), or Gaussian processes (GPs) – have not resulted in a better model [57,58].

The adsorption analysis was conducted according to Ref.[52]. The Langmuir model was used to fit the data [52]. Ninety-five percent (95%) confidence intervals are reported (if not specified otherwise).

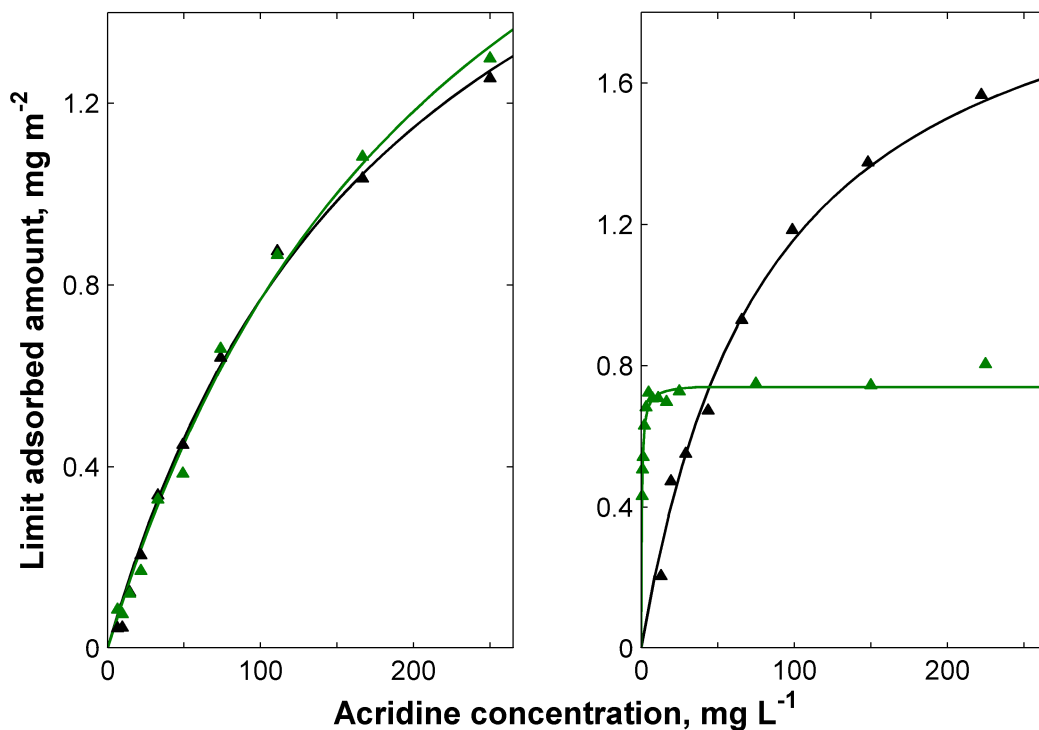


Figure 2. Thermodynamics of acridine adsorption from (left) ethanol and (right) benzene solutions onto (black) flat or (green) nanorough Au surfaces. The experimental data points were fitted with Langmuir adsorption mode.

3. RESULTS AND DISCUSSION

Figure 1 shows the kinetics of acridine adsorption onto gold from ethanol and benzene solution. One can clearly see that the surface nanoroughness does not have any effect on the ethanol data, but it dramatically effects the adsorption behavior of molecules in aromatic solvent.

The same effect is observed when thermodynamic data is measured (Figure 2). The ethanol data points are inside the confidence interval of a single Langmuir adsorption curve, while a clearly different behavior is observed for benzene solutions. The left parts of Figures 1 and 2 can also be used as a proof of the robustness of NIR-based method for studying adsorption: it shows the reproducibility of our results on different surface types. These two data sets prove that the effect observed in the case of benzene solution is not an artifact.

Table 1 summarizes the kinetic and thermodynamic data measured by near-infrared spectroscopy from different

acridine solutions. The ~70% increase of the Gibbs free energy of the adsorption process, which leads to a difference of the adsorption constants by two orders of magnitude, and the 3-fold decrease of the adsorbed amount per surface area when going from flat to nanorough Au surfaces is observed for benzene solutions. The only parameter that stays the same for both surfaces is the desorption kinetic constant.

Table 1. Thermodynamic parameters of acridine adsorption onto flat and nanorough surfaces.

Solvent / Surface type		Ethanol		Benzene	
		Flat	Nanorough	Flat	Nanorough
Maximum adsorbed amount (Γ_{\max})	mg m ⁻²	2.3±0.4	2.6±0.6	2.13±0.14	0.75±0.03
Adsorption constant (K)	M ⁻¹	930±280	770±280	(2.1±0.4)·10 ³	(3.9±0.9)·10 ⁵
Adsorption kinetic constant (k_{ads})	min ⁻¹ M ⁻¹	21±3	22±4	26±3	4160±220
Desorption kinetic constant (k_{des})	min ⁻¹	0.023±0.007	0.029±0.007	0.012±0.003	0.011±0.002
Gibbs energy of adsorption (ΔG_{ads})	kcal mol ⁻¹	-4.1±0.2	-4.0±0.2	-4.57±0.10	-7.67±0.13

The application of NIR method to acridine solution allows one to estimate the kinetic and the thermodynamic parameters of acridine adsorption onto gold (Table 1). Unfortunately, no intrinsic information on the physics or chemistry of the adsorption process is provided by this method. One cannot say anything conclusive about the origins of the difference in thermodynamic parameters for Au surfaces with different roughness from the NIR data alone.

Tip-enhanced Raman spectroscopy (TERS) is much better suited to clarify the physical and chemical details of acridine adsorption onto different gold surfaces. The possibility to get vibrational data – a direct probe of the adsorbed acridine molecular structure and the adsorption mode – makes TERS a method of choice for such a study (when compared, for example, with AFM/STM, XPS, or surface enhanced Raman spectroscopy – SERS). The possibility to study adsorbed acridine at ambient conditions (no vacuum is needed) is also a great advantage of TERS when compared with many popular surface science techniques [55,59]. Last but not least, an advantage of TERS, being a Raman-based technique, is the possibility to explore the low-frequency region of the spectrum (< 400 cm⁻¹) which is inaccessible to reflection-based infrared (ATR-FTIR) or sum frequency generation (SFG) spectroscopies. This spectral range is sensitive to intermolecular interactions and molecular adsorption bonds (“soft modes”) [63]. Together with a possibility to study submonolayers [64], it makes TERS a method of choice for many adsorption studies.

The TER spectra of adsorbed acridine on the different gold surfaces are reported in Figure 3. Note that the same experimental conditions were applied for the NIR and the TERS measurements. Comparison of the TER and the solid-state Raman spectrum clearly shows a number of changes. First, the adsorption of acridine from benzene solution onto flat gold leads to a red shift of the main Raman peaks by ~4-8 cm⁻¹. The largest shift is observed for the acridine “breathing” mode (at ~1400 cm⁻¹; confirmed by DFT calculations). A contrasting spectral behavior is seen for the molecules that are adsorbed on nanorough gold. Much smaller shifts (~2 cm⁻¹) and an appearance of an extra low-frequency band at ~195 cm⁻¹ are observed (Figure 4).

The TERS results can be interpreted as a change of the adsorption mode of acridine molecules when going from a flat to a nanorough gold surface. Relatively high red shifts are common for adsorption via π -electron cloud of aromatic

systems [33-35], while the appearance of a low-frequency band is common for adsorption via a lone electron pair (of nitrogen, in our case) with a formation a “quasi” N⁻Au chemical bond [56]. The same is valid for the surface enhanced Raman spectroscopy data. This bond is expected to be highly Raman active due to a large change in polarisability tensor during N⁻Au bond contraction (stretching).

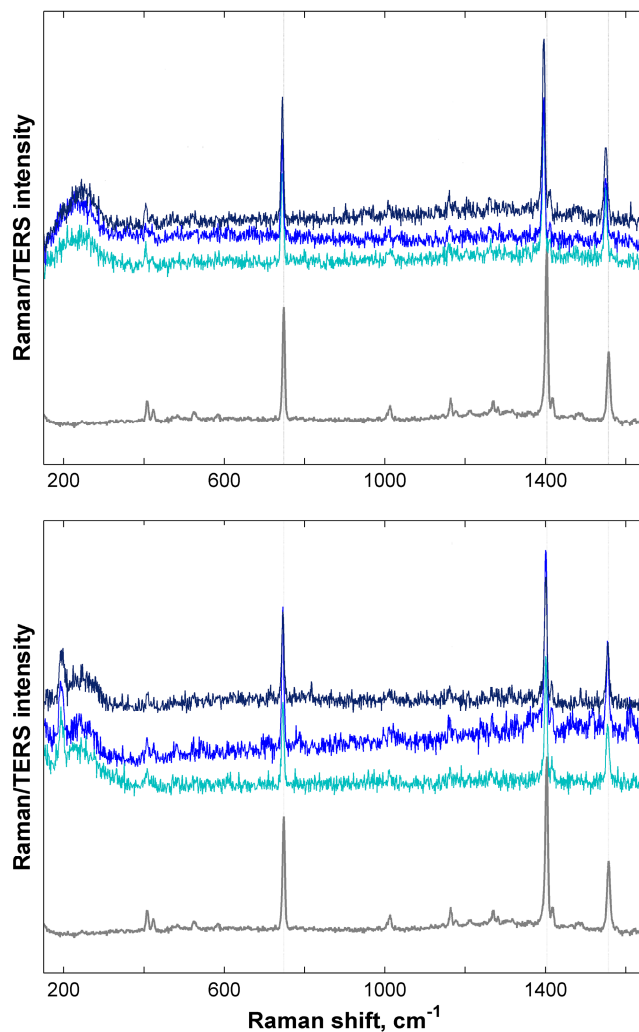


Figure 3. TERS data between 150 and 1650 cm^{-1} for acridine adsorbed onto (top) flat or (bottom) nanorough Au surfaces from benzene solution. The enhanced (blue) TER spectra of acridine submonolayer (2-3 s collection time) are presented together with (grey) solid state spectra recorded using 1 h collection time. Note the appearance of a low-frequency band at $\sim 195 \text{ cm}^{-1}$ for the molecules adsorbed onto a nanorough ($\sim 4 \text{ nm}$) surface and a relatively large (up to 8 cm^{-1}) shift of high-frequency acridine modes for the molecules adsorbed onto a flat gold surface.

Identical (flat-type) results were observed on a atomically flat gold surface. The same adsorption mode with identical adsorption parameters (Table 1) is found for atomically flat surfaces and the 50-nm coated ones. It means that no size effect is observed when gold clusters have an effective size of $\sim 20 \text{ nm}$ (see above), which is consistent with other

experimental and theoretical results [1-11].

DFT data confirm the vibrational mode assignment: the position of acridine–(gold dimer) bond is predicted to be at $\sim 200\text{ cm}^{-1}$ by different density functionals with and without the dispersion correction (B3LYP/6-31G(d), M06/6-31+G(d), M06/6-311+G(d,p), etc.) [27]. A number of other low-frequency bands is predicted to appear in the region below 300 cm^{-1} , but their experimental identification is complicated by the presence of AgO_x bands in this region (Figure 3, broad feature below 400 cm^{-1}).

The combination of three major experimental techniques, namely, near-infrared spectroscopy of acridine solution (to derive thermodynamic parameters of adsorption), tip-enhanced Raman spectroscopy of the adsorbate, and X-ray photoelectron spectroscopy of the adsorbent, leads to a clear picture of the different acridine adsorption modes on the gold “nanoparticles” of different size [38]. The fact that acridine adsorption via the nitrogen free electron pair prevails in the case of nanorough Au surface can be explained in two ways: (i) the adsorption energy of this mode increases when going from flat to rough gold, and (ii) the energy of the adsorption mode via the conjugated π -electron system decreases. Both factors can, of course, contribute to the final effect. The steric influence of the gold roughness should also not be forgotten; note that the effective size of acridine molecule is around 1.1 nm. The overlap of the π -electron cloud with gold orbitals can be disturbed by the surface nanoroughness, leading to a poorer binding of the molecule lying flat on the surface. The greater accessibility of edge gold atoms to the nitrogen lone pair [22] can result in stronger binding by this mode for non-flat samples. In other words, repulsion potential between the acridine hydrogens and the gold atoms plays a lesser role in upright acridine binding for nanorough surfaces.

The fact that ethanol solution shows no measurable effect of gold roughness should not be forgotten (Figures 1 and 2). Solvation effects seem to be of great importance for the acridine adsorption behavior. Also, that the results from different solvents should be compared with extreme care. As expected, the introduction of a polar solvent capable of forming H-bonds to an acridine system with the lone electron pair has a great effect, destroying the observed effect of surface roughness. The polarity of ethanol produces much greater intermolecular forces (higher solvation free energy) than that of benzene that makes the observed surface effects minor. One can also expect a competitive adsorption between the substance and the solvent, but Figure 2 clearly shows approximately the same acridine surface coverage for both solvents (benzene and ethanol). It suggests (but, of course, not proves) that the competition between ethanol and acridine is a minor factor to the solvent effect observed. Extra data are needed to clarify the solvation contribution to the acridine adsorption.

The change of the adsorption mode for different (aromatic) substances is expected to contribute to the enhanced catalytic activity of nanorough gold [1-11]: the change of the acridine adsorption mode changes the electronic structure of the adsorbed molecule and makes it more accessible to chemical agents (such as oxygen or hydrogen). In other words, the change in gold electronic structure has an effect on the molecule adsorption mode / behavior, which in turn leads to a change in the molecular electronic structure and chemical availability for other molecules, resulting in an enhanced chemical reactivity (a catalytic effect of AuNP). Of course, it is hard to conclude how general the proposed line of reasoning will be, having data only for acridines. Further research will be needed to clarify the applicability of this model to other chemical systems.

4. CONCLUSIONS

Adsorption of acridine from benzene solution onto gold surfaces depends on the substrate nanoroughness. Different adsorption modes of acridine molecules are observed on different gold surfaces. Acridine adsorption via the conjugated π -electron system is observed in the case of flat gold; adsorption by the nitrogen lone pair is observed on nanorough gold

(~4 nm). The difference in the adsorption behavior with a qualitative change in adsorption mode can be explained by a change of the electronic structure of gold clusters and particles when going from 4-nm to larger ones. TER spectroscopy can provide chemical information for extremely low surface coverages to clarify the behavior of surface adsorbates. A combination of near-infrared (NIR) and tip-enhanced Raman spectroscopy is found to be an effective tool to study adsorption behavior of organic molecules from both, thermodynamic and molecular, points of views. Here we made only one step towards a detailed understanding of the role of nanoscale effects in gold catalytic activity.

REFERENCES

- [1] Editorial, *Nat. Nanotechnol.*, 2008, 3, 575.
- [2] M. D. Hughes, et al., *Nature*, 2005, 437, 1132.
- [3] D. J. Gorin, F. D. Toste, *Nature*, 2007, 446, 395.
- [4] Z. Y. Li, et al., *Nature*, 2008, 451, 46.
- [5] V. Lavallo, G. D. Frey, S. Kousar, B. Donnadieu, G. Bertrand, *Proc. Natl. Acad. Sci. USA*, 2007, 104, 13569–13573;
- [6] C. H. Christensen, J. K. Nørskov, *Science*, 2010, 327, 278.
- [7] B. N. Zope, D. D. Hibbitts, M. Neurock, R. J. Davis, *Science*, 2010, 330, 74.
- [8] L. Gross, F. Mohn, P. Liljeroth, J. Repp, F. J. Giessibl, G. Meyer, *Science*, 2009, 324, 1428.
- [9] A. Wittstock, et al., *Science*, 2010, 327, 319.
- [10] R. M. Balabin, *J. Phys. Chem. A*, 2009, 113, 4910.
- [11] R. Olson, S. Varganov, M. S. Gordon, H. Metiu, *Chem. Phys. Lett.*, 2005, 412, 416–419.
- [12] T. Hayashi, K. Tanaka, M. Haruta, *J. Catal.*, 1998, 178, 566.
- [13] F. C. Meunier, *ACS Nano*, 2008, 1, 2441–2444.
- [14] M. Turner, *Nature*, 2008, 454, 981.
- [15] Y. Wei, *Angew. Chem. Int. Ed.*, 2011, 50, 2326–2329.
- [16] M. Valden, X. Lai, D. W. Goodman, *Science*, 1998, 281, 1647–1650.
- [17] A. Roldán, S. González, J. M. Ricart, F. Illas, *ChemPhysChem*, 2009, 10, 348–351.
- [18] Y. Pei, N. Shao, Y. Gao, X. C. Zeng, *ACS Nano*, 2010, 4, 2009–2020.
- [19] T. Fujitani, I. Nakamura, T. Akita, M. Okumura, M. Haruta, *Angew. Chem. Int. Ed.*, 2009, 48, 9515–9518.
- [20] B. Hammer, J. K. Nørskov, *Nature*, 1995, 376, 238–240.
- [21] E. Bus, J. T. Miller, J. A. van Bokhoven, *J. Phys. Chem. B*, 2005, 109, 14581–14587.
- [22] R. M. Balabin, R. Z. Safieva, *Energy Fuels*, 2011, 25, 2373.
- [23] Y. Pan, A. Leifert, D. Ruau, S. Neuss, J. Bornemann, G. Schmid, W. Brandau, U. Simon, W. Jahn-Dechent, *Small*, 2009, 5, 2067–2076.
- [24] H. Zhu, X. Ke, X. Yang, S. Sarina, H. Liu, *Angew. Chem. Int. Ed.*, 2010, 49, 9657–9661.
- [25] J. Boscoboinik, J. Kestell, M. Garvey, M. Weinert, W. T. Tysse, *Top. Catal.*, 2011, 54, 20–25.
- [26] A. Griprane, A. Corma, H. García, *Science*, 2008, 322, 1661.
- [27] W. T. Wallace, R. L. Whetten, *J. Am. Chem. Soc.*, 2002, 124, 7499–7505.
- [28] F. Boccuzzi, A. Chiorino, M. Manzoli, *Materials Science and Engineering C*, 2001, 15, 215–217.
- [29] R. M. Balabin, E. I. Lomakina, *Analyst*, 2011, 136, 1703.
- [30] M. Haruta, S. Tsubota, T. Kobayashi, H. Kageyama, M. J. Genet, B. Delmon, *J. Catal.*, 1993, 144, 175.
- [31] W. T. Wallace, R. L. Whetten, *J. Phys. Chem. B*, 2000, 104, 10964.
- [32] A. Corma, A. Leyva-Pérez, M. J. Sabater, *Chem. Rev.*, 2011, 111, 1657–1712.
- [33] J. Huang, T. Akita, J. Faye, T. Fujitani, T. Takei, M. Haruta, *Angew. Chem. Int. Ed.*, 2009, 48, 7862.

- [34] T. A. Nijhuis, E. Sacaliuc, A. M. Bealeb, A. M. J. van der Eerden, J. C. Schouten, B. M. Weckhuysen, *J. Catal.*, 2008, 258, 256.
- [35] S. Lee, L. M. Molina, M. J. Lopez, J. A. Alonso, B. Hammer, B. Lee, S. Seifert, R. E. Winans, J. W. Elam, M. J. Pellin, S. Vajda, *Angew. Chem. Int. Ed.*, 2009, 48, 1467.
- [36] A. Roldan, D. Torres, J. M. Ricart, F. Illas, *J. Mol. Catal. A: Chem.*, 2009, 306, 6.
- [37] Y. Xiang, Q. Meng, X. Li, J. Wang, *Chem. Commun.*, 2010, 46, 5918–5920.
- [38] H. Wu, L. Wang, J. Zhang, Z. Shen, J. Zhao, *Catalysis Communications*, 2011, 12, 859–865.
- [39] R. M. Balabin, R. Z. Syunyaev, T. Schmid, J. Stadler, E. I. Lomakina, R. Zenobi, *Energy Fuels*, 2011, 25, 189.
- [40] R. M. Balabin, R. Z. Syunyaev, *J. Colloid Interf. Sci.*, 2008, 318, 167.
- [41] R. M. Balabin, S. V. Smirnov, *Anal. Chem. Acta*, 2001, 692, 63.
- [42] J. Stadler, T. Schmid, R. Zenobi, *Nano Lett.*, 2010, 10, 4514–4520.
- [43] S. Brunauer, P. H. Emmett, E. Teller, *J. Am. Chem. Soc.*, 1938, 60, 309.
- [44] R. M. Balabin, E. I. Lomakina, *Phys. Chem. Chem. Phys.*, 2011, 13, 11710.
- [45] R. M. Balabin, *J. Phys. Chem. A*, 2009, 113, 1012.
- [46] A. K. Santra, D. W. Goodman, *J. Phys.: Condens. Matter*, 2002, 14, R31–R62.
- [47] K. Takahiro, et al., *J. Appl. Phys.*, 2006, 100, 084325.
- [48] L. K. Ono, D. Sudfeld, B. R. Cuenya, *Surface Science*, 2006, 600, 5041–5050.
- [49] R. M. Stockle, Y. D. Suh, V. Deckert, R. Zenobi, *Chem. Phys. Lett.*, 2000, 318, 131–136.
- [50] A. Davydov, *Molecular Spectroscopy of Oxide Catalyst Surfaces*, Wiley, 2003, 690.
- [51] B. Pettinger, B. Ren, G. Picardi, R. Schuster, G. Ertl, *Phys. Rev. Lett.*, 2004, 92, 096101.
- [52] T. C. Dinadayalane, J. Leszczynski, *J. Chem. Phys.*, 2009, 130, 081101.
- [53] R. M. Balabin, E. I. Lomakina, R. Z. Safieva, *Fuel*, 2011, 90, 2007.
- [54] J. Creighton, C. Blatchford, M. Albrecht, *J. Chem. Soc.: Faraday Trans.*, 1979, 75, 790.
- [55] K. Barylyuk, R. M. Balabin, D. Grünstein, R. Kikkeri, V. Frankevich, P. H. Seeberger, R. Zenobi, *J. Am. Soc. Mass Spectrom.*, 2011, 22, 1167.
- [56] R. M. Balabin, S. V. Smirnov, *Talanta*, 2011, 85, 562.
- [57] R. M. Balabin, R. Z. Safieva, *Anal. Chim. Acta*, 2011, 689, 190.
- [58] R. M. Balabin, R. Z. Safieva, E. I. Lomakina, *Microchem. J.*, 2011, 98, 121.
- [59] T. Chen, H. Wang, G. Chen, Y. Wang, Y. Feng, W. S. Teo, T. Wu, H. Chen, *ACS Nano*, 2010, 4, 3087–3094.